



Contents lists available at ScienceDirect

Digital Communications and Networks

journal homepage: www.keaipublishing.com/dcan

Spectrum and energy efficient multi-antenna spectrum sensing for green UAV communication

Junlin Zhang^a, Mingqian Liu^{a,*}, Nan Zhao^b, Yunfei Chen^c, Qinghai Yang^a, Zhiguo Ding^d^a State Key Laboratory of Integrated Service Networks, Xidian University, Shaanxi, Xi'an, 710071, China^b School of Information and Communication Engineering, Dalian University of Technology, Dalian, 116024, China^c Department of Engineering, University of Durham, Durham, DH1 3LE, UK^d School of Electrical and Electronic Engineering, University of Manchester, Manchester, UK

ARTICLE INFO

Keywords:

Green communication
Multi-antenna spectrum sensing
Non-Gaussian noise
Unmanned aerial vehicle communication

ABSTRACT

Unmanned Aerial Vehicle (UAV) communication is a promising technology that provides swift and flexible on-demand wireless connectivity for devices without infrastructure support. With recent developments in UAVs, spectrum and energy efficient green UAV communication has become crucial. To deal with this issue, Spectrum Sharing Policy (SSP) is introduced to support green UAV communication. Spectrum sensing in SSP must be carefully formulated to control interference to the primary users and ground communications. In this paper, we propose spectrum sensing for opportunistic spectrum access in green UAV communication to improve the spectrum utilization efficiency. Different from most existing works, we focus on the problem of spectrum sensing of randomly arriving primary signals in the presence of non-Gaussian noise/interference. We propose a novel and improved p -norm-based spectrum sensing scheme to improve the spectrum utilization efficiency in green UAV communication. Firstly, we construct the p -norm decision statistic based on the assumption that the random arrivals of signals follow a Poisson process. Then, we analyze and derive the approximate analytical expressions of the false-alarm and detection probabilities by utilizing the central limit theorem. Simulation results illustrate the validity and superiority of the proposed scheme when the primary signals are corrupted by additive non-Gaussian noise and arrive randomly during spectrum sensing in the green UAV communication.

1. Introduction

Unmanned Aerial Vehicles (UAVs) are attracting increasing attention to provide an on-demand flexible platform for deploying aerial base stations or installing mobile access points [1,2]. UAV communication is promising for many applications, such as surveillance, emergency response, internet of things, public safety and transportation [3–5]. Recently, spectrum-efficient and energy-efficient green UAV communication has attracted much attention [6,7]. To improve the spectrum efficient, spectrum sharing is introduced into UAV communications to increase the UAVs' available radio resources [8]. Moreover, spectrum sharing can reduce the overhead and energy consumption of UAV as relays. Spectrum sensing plays a critical role in spectrum sharing. It can detect available spectrum resources to avoid interferences to the Primary Users (PUs). Unlike previous communication networks, spectrum sensing faces many new challenges in green UAV communication. One of the

critical challenges is the highly dynamic characteristics of Air-To-Ground (ATG) channels [9]. The propagation characteristics of ATG channels depend on the UAV flight dynamics, including the altitude, distance and elevation angle. Another challenge is the concern about sensing efficiency when considering the impairment of various types of non-Gaussian noise/interference, such as human-made impulsive noise and co-channel interference. It is necessary to achieve a higher detection rate, lower false alarm probability and lower missing detection probability in the presence of non-Gaussian noise/interference.

Spectrum sensing is one of the main components spectrum sharing. In the literature, various spectrum sensing methods have been proposed for impairment by Additive White Gaussian Noise (AWGN), which include Matched Filter detector (MF) [10], the Energy Detector (ED) [11], Cyclostationarity-based Detector (CD) [12], Eigenvalue-based Detector (EVD) [13] and Covariance-based Detector (CVD) [14], etc. These methods have advantages and disadvantages. MF and ED could achieve

* Corresponding author.

E-mail addresses: zhangjunlin@xidian.edu.cn (J. Zhang), mqliu@mail.xidian.edu.cn (M. Liu), zhaonan@dlut.edu.cn (N. Zhao), Yunfei.Chen@durham.ac.uk (Y. Chen), qhyang@xidian.edu.cn (Q. Yang), zhiguo.ding@manchester.ac.uk (Z. Ding).<https://doi.org/10.1016/j.dcan.2022.09.017>

Received 25 September 2021; Received in revised form 20 July 2022; Accepted 21 September 2022

Available online 5 October 2022

2352-8648/© 2022 Chongqing University of Posts and Telecommunications. Publishing Services by Elsevier B.V. on behalf of KeAi Communications Co. Ltd. This is an open access article under the CC BY-NC-ND license (<http://creativecommons.org/licenses/by-nc-nd/4.0/>).

optimal performance while requiring perfect knowledge of primary signals. CD provides high accuracy, but it has high computational complexity. EVD and CVD could achieve relatively outstanding performance without any prior information, but their performance could not be guaranteed in a complex channel environment. Moreover, several methods have been presented to ameliorate the performance of spectrum sensing in the presence of non-Gaussian, such as Fractional Lower Order Moment (FLOM) based detector [15], p -norm detector [16,17] and Polarity-Coincidence-Array (PCA) detector [18,19]. FLOM-based detector could achieve a significant performance enhancement in the α -stable distributed noise, but this detector required knowledge of the power of the primary signals. The p -norm detector could achieve lower false alarm probability and false dismissal probability in generalized Gaussian noise and Gaussian mixture noise. This detector required statistical information about the primary signal and channel. PCA detector could outperform the ED scheme for generalized Gaussian noise, but its performance was dependent on the parameters of softness. Most of these works assume that primary signals maintain constant occupancy during the sensing period. In practical scenarios, primary signals may arrive anytime during the frame when PUs traffic is heavy or Secondary User (SU) frame duration is long, which will lead to high miss detection probability. Spectrum sensing methods under the condition of random arrivals of PU have been addressed by several researchers recently. Beaulieu et al. proposed the Generalized Likelihood Ratio Test (GLRT) detector for randomly arriving PUs [20]. In Ref. [21], a new weighted scheme based on cumulative sum was presented for detecting primary signals when primary signals arrive randomly during the sensing period. In Ref. [22], Chin et al. proposed a low-complexity GLRT based on the energy method to improve the detection performance under the condition of random arrivals of PUs. Deng et al. designed an adaptive weighted energy detection based on power function in the dynamic PU traffic environment [23]. In Ref. [24], Wang et al. adopted the Poisson model to characterize the random arrival process of primary signals and proposed Multiple-Antenna Linearly Weighted (MALW) method. The method constructed the total test statistic by linearly combining a weighted local test statistics.

In this paper, we focus on the study of spectrum sensing for UAV communication, which could detect available spectrum resources in UAV communication and avoid interferences between secondary users and nearby primary users. Few research works have been conducted on spectrum sensing for UAV communication. In Ref. [25], Xu et al. proposed a new compressive signal processing-based algorithm for wide-band spectrum sensing in UAV communication. In Ref. [26], Shen et al. presented a three-dimensional spatiotemporal sensing framework for joint spatio-temporal spectrum sensing by using the flexibility of UAV spectrum sensors. Liu et al. in Ref. [27] developed a UAV-aided detector to improve spectrum sensing performance in the LOS channel. Moreover, in Refs. [28–30], spectrum sensing was employed to protect the PU from harmful interference in the UAV communications.

To the best of our knowledge, no work has yet considered the issue of spectrum sensing with random arrivals of primary signals in the presence of impulsive noise for UAV communication. This motivates us to improve the performance of spectrum sensing for UAV communication by designing a novel p -norm-based detector for the detection of primary signals when primary signals are corrupted by additive non-Gaussian noise and arrive randomly during the spectrum sensing period over mixed LoS/non LoS (NLoS) channel. The main contributions of this paper are summarized as follows:

- We investigate the application of spectrum sharing in UAV communication, focusing on the spectrum sensing. A novel p -norm-based detector is proposed for UAV communication, which can efficiently detect primary signals with random arrivals in the presence of non-Gaussian noise.
- Different from most existing works, we study the spectrum sensing with random arrivals of primary signals in the presence of non-

Gaussian noise for UAV communication. We adopt Poisson model to characterize the random arrival process of primary signals and employ three models of non-Gaussian noise, which include the alpha-stable distribution, the Generalized Gaussian Distribution (GGD) and the Gaussian Mixture Distribution (GMD).

- We analyze and derive asymptotic expressions of the detection and false alarm probabilities for the proposed p -norm-based detector in the presence of non-Gaussian noise in UAV communication.

The rest of the paper is organized as follows. Section 2 presents the detailed description of system model, channel model and noise model. In Section 3, the p -norm-based sensing scheme is introduced for UAV communication. The theoretical performance of the proposed detector is analyzed in Section 4. Our numerical results are provided in Section 5 for verifying our analysis. Finally, the concluding remarks are presented in Section 6.

2. System model

In this section, we present the system model for the proposed scheme.

2.1. System structure

As shown in Fig. 1, we consider a system where secondary users need to share the same frequency resource of green UAV communication with PUs. The system consists of a Primary Transmitter (PT), a Primary Receiver (PR), a multi-antenna UAV and an SU. The UAV is deployed to provide wireless connections for PUs without reliable direct communication links on the ground. When the primary communication is performed, the data are transmitted from the PT to PR in two steps. In the first step, the PT sends data directly to the multi-antenna UAV. In the second step, the data are received by the multi-antenna UAV, which is retransmitted to the PR through UAV. The PUs, i.e., PT and PR, have the priority to use the licensed spectrum of UAV communication. The SU is allowed to access the licensed spectrum with the help of UAV only if the licensed spectrum is idle. In order to reduce the communication interference caused by the SU, the SU should perform spectrum sensing to acquire the state of licensed spectrum, i.e., idle or busy. In this paper, we assume that the direct communication link between the SU and the PT does not exist. The SU needs to determine the signal from the UAV to detect the state of the licensed spectrum. Assume that the UAV's coverage is circular with a radius of R , and the UAV is located at the center of the

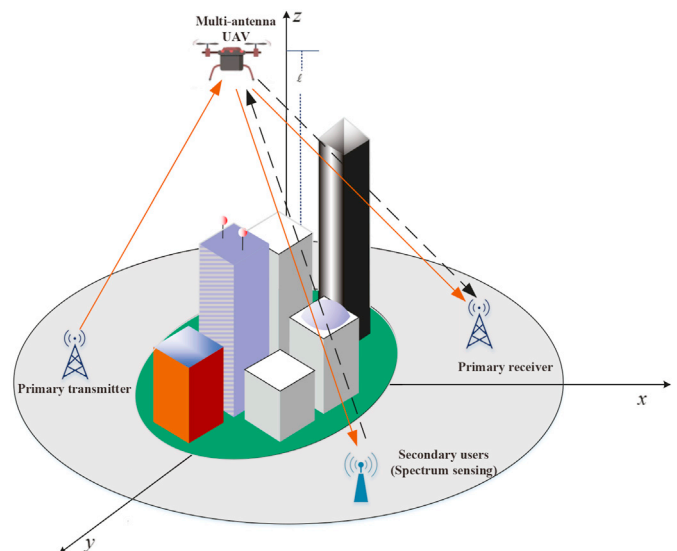


Fig. 1. System model of spectrum sensing for green UAV communication.

disc. The height of UAV is ℓ , and the horizontal distance between SU and UAV projection is r .

In the spectrum sensing, the SU needs to detect if the signal from UAV exists or not, so as to determine whether the licensed spectrum is idle or busy. We consider the UAV with Q antennas and an SU with K antennas. The problem of spectrum sensing with random arrivals of primary signal can be formulated as

$$\begin{cases} x_k(n) = w_k(n) & n = 1, 2, \dots, N & \mathcal{H}_0 \\ x_k(n) = \begin{cases} w_k(n) & n = 1, 2, \dots, J \\ \sum_{q=1}^Q g_{kq}s_q(n) + w_k(n) & n = J + 1, \dots, N \end{cases} & \mathcal{H}_1 \end{cases} \quad (1)$$

where $x_k(n)$ denotes the n -th received sample from the k -th receiving antenna and $s_q(n)$ represents the n -th samples of the primary signals from the q -th transmitting antenna of the UAV. g_{kq} denotes the channel coefficient between the q -th antenna of the UAV and the k -th antenna of SU, $w_k(n)$ stands for the additive non-Gaussian noise, N is the number of samples, $J + 1$ denotes the arrival time of the UAV signal and the value of J is between 0 and $N - 1$. Poisson Process (PP) is widely used for modeling the arrival process of the signal. Therefore, we adopt a PP with the arrival rate λ to model the UAV signal.

2.2. Channel model

The ATG propagation channel experiences both path loss and small-scale fading. The LoS link between UAV and ground receiver may be blocked by potential obstacles, such as buildings. The ATG channel is composite LoS/Non-LoS (NLoS) channel model [31,32]. The probabilistic LoS and NLoS model is expressed as

$$\xi(d) = \begin{cases} \psi_L d_{su}^{-\Delta_L} \text{LoS link with prob.} \\ \psi_N d_{su}^{-\Delta_N} \text{NLoS link with prob.} \end{cases} \quad (2)$$

where ψ_L and ψ_N are the path loss exponents of the LoS link and NLoS link, respectively. d_{su} stands for the distance between the UAV and SU with $d_{su} = \sqrt{\ell^2 + r^2}$ p_L and p_N are LoS probability and NLoS probability of the G2A channels, respectively, and $p_N = 1 - p_L$. The probability of having LoS is given by

$$p_L(d_{su}, \ell) = (1 + Ae^{-B(\zeta-A)})^{-1} \quad (3)$$

where ζ denotes an elevation angle of the SU with respect to the UAV and $\zeta = \arcsin(\frac{\ell}{d_{su}})$. A and B are environment (rural, urban, dense urban, etc.) dependent constants. For the small-scale fading, the Nakagami- m distribution is applied to the random multipath fading [33]. The small-scale fading matrix from the UAV to SU can be defined as

$$\mathbf{H} = \begin{bmatrix} h_{11} & \dots & h_{1Q} \\ \vdots & \ddots & \vdots \\ h_{K1} & \dots & h_{KQ} \end{bmatrix} \quad (4)$$

where \mathbf{H} is the channel matrix containing $K \times Q$ elements. The envelope of h follows the Nakagami- m distribution and the phase is known to be non-uniformly distributed. The density function of the channel gain $|h|^2$ is $f_{|h|^2}(y) = \frac{m^m}{\Omega^m \Gamma(m)} y^{m-1} e^{-\frac{my}{\Omega}}$, where $\Gamma(\cdot)$ denotes the gamma function, and m and Ω are shape and scale parameters, respectively.

2.3. Noise model

In practical systems, there are many situations for which the underlying noise model does not fit a Gaussian model, such as man-made

impulsive noise, co-channel interference, out-of-band spectral leakage, and interference from ultra-wideband systems. In particular, the non-Gaussian noise is caused by the co-channel interference which occurs within UAV communications or between ground communication with the lack of a dedicated spectrum. Currently, several models are considered to fit the non-Gaussian noise or interference in the literature. The most popular models for the non-Gaussian noise are GMD, GGD and alpha-stable distribution.

2.3.1. Gaussian mixture noise (GMN) model

GMN is often used to describe the man-made impulsive and atmospheric interference [34]. The tail of the Probability Density Function (P.D.F.) of GMN is heavier than the Gaussian distribution, and a heavier tail usually represents a larger degree of impulsive. The P.D.F. of the GMN can be expressed as

$$f(w_k) = \sum_{i=1}^U \frac{b_i}{\sqrt{2\pi\sigma_i^2}} \exp\left(-\frac{w_k^2}{2\sigma_i^2}\right) \quad (5)$$

where $b_i > 0$ is the mixing weight of GMN and $\sum_{i=1}^U b_i = 1$. σ_i^2 is the variance of the noise component and U is the number of the components in the GMN. When $U = 1$, GMN stands for a Gaussian noise. The variance of the GMN is $\sigma_w^2 = \sum_{i=1}^U b_i \sigma_i^2$.

2.3.2. Generalized Gaussian noise (GGN) model

GGN model is also used to characterize the non-Gaussian noise [35]. The P.D.F. of which can be given by

$$f(w_k) = \frac{1}{2\Gamma(\frac{1}{\beta})A(\beta, \sigma_w)} \exp\left(-\left|\frac{w_k}{A(\beta, \sigma_w)}\right|^\beta\right) \quad (6)$$

where

$$A(\beta, \sigma_w) = \sqrt{\sigma_w^2 \Gamma(1/\beta) / \Gamma(3/\beta)}$$

and β is the shape parameter, which can be used to control the heaviness of the tails of non-Gaussian. Laplacian noise and Gaussian noise are contained in GGN as special cases when $\beta = 1$ and $\beta = 2$, respectively.

2.3.3. Alpha-stable noise (ASN) model

The ASN model has no closed-form expression of the P.D.F., and can be described by its characteristic function as

$$\varphi(\zeta) = \exp\{je\zeta - \gamma|\zeta|^\alpha [1 + j\eta \text{sgn}(\zeta)\omega(\zeta, \alpha)]\} \quad (7)$$

where

$$\omega(\zeta, \alpha) = \begin{cases} \tan(\pi\alpha/2) & \alpha \neq 1 \\ (2/\pi)\log|\zeta| & \alpha = 1 \end{cases} \quad (8)$$

$$\text{sgn}(\zeta) = \begin{cases} 1 & \zeta > 0 \\ 0 & \zeta = 0 \\ -1 & \zeta < 0 \end{cases} \quad (9)$$

and α represents the characteristic exponent, e denotes the location parameter, γ is the dispersion parameter and η stands for the index of skewness. When the stable distribution is symmetric with $\eta = 0$, the characteristic function $\varphi(t)$ is reduced to $\varphi(\zeta) = \exp\{je\zeta - \gamma|u|^\alpha\}$. Two well-known special distributions are Cauchy distribution ($\alpha = 1$) and Gaussian distribution ($\alpha = 2$) [15].

3. Improved p -norm-based spectrum sensing scheme

In this section, we propose a novel p -norm-based spectrum sensing scheme for randomly arriving primary signals under non-Gaussian noise in UAV communications.

When the state of PU does not change during spectrum sensing, the optimal decision statistic can be expressed as

$$\Lambda_{\text{OP}} = \log \frac{f_{\mathcal{X}\mathcal{H}}(\mathbf{x}|\mathcal{H}_1)}{f_{\mathcal{X}\mathcal{H}}(\mathbf{x}|\mathcal{H}_0)} = \log \left(\prod_{k=1}^K \prod_{n=1}^N \frac{f_{w_k}(x_k(n) - \tilde{s}_k(n))}{f_{w_k}(x_k(n))} \right) \quad (10)$$

where $\mathbf{x} = [x_1(n), \dots, x_M(n)]^T$ is a vector of observations $x_k(n)$ and $f_{\mathcal{X}\mathcal{H}}(\mathbf{x}|\mathcal{H}_i)$ represents the probability density function of \mathbf{x} conditioned on \mathcal{H}_i for $i = 0, 1$. For AWGN, the corresponding locally optimum detector can be expressed as

$$\Lambda_{\text{LOP}} = \sum_{k=1}^K \sum_{n=1}^N |x_k(n)|^2 \quad (11)$$

As mentioned in Section 2, the primary signals may arrive randomly during the sensing period. An efficient strategy for detecting randomly arriving primary signals is to model the arrival as a PP and takes it into account [20]. Based on [24], the test statistic of random arrivals of primary signals can be expressed as

$$\Lambda_{\text{LOP}} = \sum_{k=1}^K \left(\sum_{n=1}^N (1 - e^{-\lambda n}) |x_k(n)|^2 \right) \quad (12)$$

From (12), we can observe that the test statistic of the random arrivals of primary signals is the improved energy detector under the Gaussian noise assumption. Unfortunately, the presence of heavy-tailed impulsive noise degrades the performance of the energy detector. According to Ref. [15], p -norm metric ensures that the heavy-tailed impulsive noise exhibits finite absolute moments. The p -norm detector has a vast performance gain over the energy detector in both heavy-tailed and short-tailed noise [16]. Adopting p -norm metric in the proposed scheme, the improved p -norm-based test statistic can be derived as

$$\mathcal{T}_{\text{SO}} = \sum_{k=1}^K \varpi_k \exp \left(-\frac{1}{Nc} \sum_{n=1}^N (1 - e^{-\lambda n}) |x_k(n)|^p \right) \quad (13)$$

where $p > 0$ is an arbitrary constant, $c > 0$ is an arbitrary constant and ϖ_k is the weight factor.

When \mathcal{H}_0 holds, or the primary signals are not present, the test statistic \mathcal{T}_{SO} approximately follows Gaussian distribution for sufficiently large N . Thus, given false alarm probability \mathcal{P}_f , the test threshold of the proposed improved p -norm-based detection scheme in non-Gaussian noise can be set as

$$\Psi = \mathbb{Q}^{-1}(1 - \mathcal{P}_f) \sqrt{\mathbb{V}\{\mathcal{T}_{\text{SO}}|\mathbf{H}_0\}} + \mathbb{E}\{\mathcal{T}_{\text{SO}}|\mathbf{H}_0\} \quad (14)$$

where $\mathbb{Q}^{-1}(\cdot)$ is the inverse function of $\mathbb{Q}(\cdot)$, $\mathbb{Q}(t) = (1/\sqrt{2\pi}) \int_t^\infty e^{-u^2/2} du$. $\mathbb{V}\{\mathcal{T}_{\text{SO}}|\mathbf{H}_0\}$ and $\mathbb{E}\{\mathcal{T}_{\text{SO}}|\mathbf{H}_0\}$ represent the variance and mean of the test statistic \mathcal{T}_{SO} under the \mathcal{H}_0 hypothesis, respectively.

Therefore, we can compare the test statistic \mathcal{T}_{SO} with the detection threshold Ψ to determine if the primary signals exist or not. If $\mathcal{T}_{\text{SO}} < \Psi$, we make the decision that the primary signals are present; otherwise, the primary signals are absent. The decision rule can be given by

$$\begin{cases} \mathcal{H}_0 : \mathcal{T}_{\text{SO}} \geq \Psi \\ \mathcal{H}_1 : \mathcal{T}_{\text{SO}} < \Psi \end{cases} \quad (15)$$

The detailed algorithm steps of the improved p -norm-based detection algorithm are summarized in Algorithm 1.

Algorithm 1 Improved p -norm-based spectrum sensing scheme

- 1: Initialize parameters p and \mathcal{P}_f ;
 - 2: Compute the test statistical \mathcal{T}_{SO} ,

$$\mathcal{T}_{\text{SO}} = \sum_{k=1}^K \varpi_k \exp \left(-\frac{1}{Nc} \sum_{n=1}^N (1 - e^{-\lambda n}) |x_k(n)|^p \right),$$
 - 3: Determine a detection threshold Ψ ,

$$\Psi = \mathbb{Q}^{-1}(1 - \mathcal{P}_f) \sqrt{\mathbb{V}\{\mathcal{T}_{\text{SO}}|\mathcal{H}_0\}} + \mathbb{E}\{\mathcal{T}_{\text{SO}}|\mathcal{H}_0\},$$
 where \mathcal{P}_f is the given false alarm probability;
 - 4: Decision: if $\mathcal{T}_{\text{SO}} < \Psi$, we declare that the primary signals are present; otherwise, we declare that the primary signals are absent.
-

4. Spectrum sensing performance analysis

In this section, we evaluate the performance of the proposed improved p -norm-based detection algorithm for non-Gaussian noise. An approximate analytical expression for the false alarm probability \mathcal{P}_f and detector probability \mathcal{P}_d is derived by providing the moment of the improved p -norm-based test statistic \mathcal{T}_{SO} in the presence of GMN, GGN and ASN.

4.1. False alarm probability and test threshold

To make the problem analytically tractable, we assume that the number of samples is sufficiently large so that the central limit theorem holds. As a result, we model the decision statistic \mathcal{T}_{SO} as a Gaussian random variable under \mathcal{H}_0 hypothesis. Let

$$\mathcal{T}_{\text{SO}}|\mathbf{H}_0 = \sum_{k=1}^K \varpi_k \exp \left(-\frac{1}{Nc} \sum_{n=1}^N (1 - e^{-\lambda n}) |w_k(n)|^p \right) = \sum_{k=1}^K \varpi_k \mathcal{T}_k \mathcal{H}_0 \quad (16)$$

$$\text{where } \mathcal{T}_k \mathcal{H}_0 = \exp \left(-\frac{1}{Nc} \sum_{n=1}^N (1 - e^{-\lambda n}) |w_k(n)|^p \right).$$

We first derive the mean and variance of the test statistic $\mathcal{T}_k|\mathcal{H}_0$ under \mathcal{H}_0 . Let $|\mathcal{T}_k|\mathbf{H}_0 = \frac{1}{N} \sum_{n=1}^N (1 - e^{-\lambda n}) |w_k(n)|^p$, $\mathbb{E}\{\mathcal{T}_k|\mathcal{H}_0\}$ and $\mathbb{V}\{\mathcal{T}_k|\mathcal{H}_0\}$ can be expressed as

$$\begin{aligned} \mathbb{E}\{\mathcal{T}_k|\mathcal{H}_0\} &= \mathbb{E} \left\{ \exp \left(-\frac{1}{Nc} \sum_{n=1}^N (1 - e^{-\lambda n}) |w_k(n)|^p \right) \right\} \\ &= \exp \left(\frac{\mathbb{V}\{\mathcal{T}_k|\mathcal{H}_0\}}{2c^2} - \frac{\mathbb{E}\{\mathcal{T}_k|\mathcal{H}_0\}}{c} \right) \end{aligned} \quad (17)$$

$$\begin{aligned} \mathbb{V}\{\mathcal{T}_k|\mathbf{H}_0\} &= \mathbb{E}\{\mathcal{T}_k|\mathbf{H}_0\}^2 - (\mathbb{E}\{\mathcal{T}_k|\mathbf{H}_0\})^2 \\ &= \exp \left(\frac{\mathbb{V}\{\mathcal{T}_k|\mathbf{H}_0\}}{c^2} - \frac{2\mathbb{E}\{\mathcal{T}_k|\mathbf{H}_0\}}{c} \right) \\ &\quad \times \left(\exp \left(\frac{\mathbb{V}\{\mathcal{T}_k|\mathbf{H}_0\}}{c^2} \right) - 1 \right) \end{aligned} \quad (18)$$

Proposition 1. Denote the first and second order moment of the random variables $|w_k(n)|^p$ by $\mathcal{M}_w(p)$ and $\mathcal{M}_w(2p)$. Then, the mean and variance of

$\mathcal{F}_k|\mathcal{H}_0$ can be given by

$$\mathbb{E}\{\mathcal{F}_k|\mathbf{H}_0\} = \frac{1}{N} \left(N - \frac{e^{-\lambda} - e^{-\lambda(N+1)}}{1 - e^{-\lambda}} \right) \mathcal{M}_w(p) \tag{19}$$

$$\mathbb{V}\{\mathcal{F}_k|\mathcal{H}_0\} = \frac{1}{N^2} \left(N + \frac{e^{-2\lambda} - e^{-2\lambda(N+1)}}{1 - e^{-2\lambda}} - 2 \frac{e^{-\lambda} - e^{-\lambda(N+1)}}{1 - e^{-\lambda}} \right) \times (\mathcal{M}_w(2p) - \mathcal{M}_w^2(p)) \tag{20}$$

Proof.

According to the system model and the test statistic, the mean of \mathcal{F}_k can be computed as

$$\begin{aligned} \mathbb{E}\{\mathcal{F}_k|\mathcal{H}_0\} &= \mathbb{E}\left\{ \frac{1}{N} \sum_{n=1}^N (1 - e^{-\lambda n}) |w_k(n)|^p \right\} \\ &= \frac{1}{N} \left(N - \frac{e^{-\lambda} - e^{-\lambda(N+1)}}{1 - e^{-\lambda}} \right) \mathbb{E}\{|w_k(n)|^p\} \\ &= \frac{1}{N} \left(N - \frac{e^{-\lambda} - e^{-\lambda(N+1)}}{1 - e^{-\lambda}} \right) \mathcal{M}_w(p) \end{aligned} \tag{21}$$

where $\mathcal{M}_w(p) = \mathbb{E}\{|w_k(n)|^p\}$. The variance of \mathcal{F}_k can be calculated as

$$\begin{aligned} \mathbb{V}\{\mathcal{F}_k|\mathbf{H}_0\} &= \mathbb{V}\left\{ \frac{1}{N} \sum_{n=1}^N (1 - e^{-\lambda n}) |x_k(n)|^p \right\} \\ &= \frac{1}{N^2} \left(N + \frac{e^{-2\lambda} - e^{-2\lambda(N+1)}}{1 - e^{-2\lambda}} - 2 \frac{e^{-\lambda} - e^{-\lambda(N+1)}}{1 - e^{-\lambda}} \right) \\ &\quad \times \mathbb{V}\{|x_k(n)|^p\} \\ &= \frac{1}{N^2} \left(N + \frac{e^{-2\lambda} - e^{-2\lambda(N+1)}}{1 - e^{-2\lambda}} - 2 \frac{e^{-\lambda} - e^{-\lambda(N+1)}}{1 - e^{-\lambda}} \right) \\ &\quad \times (\mathcal{M}_w(2p) - \mathcal{M}_w^2(p)) \end{aligned} \tag{22}$$

□

Lemma 1 provides the mean and the variance of \mathcal{F}_k under \mathcal{H}_0 . The first and second moments of $|w_k(n)|^p$ are required in (19) and (20) in the presence of non-Gaussian noise. $\mathcal{M}_w(p)$ and $\mathcal{M}_w(2p)$ are provided in Lemma 1 - Lemma 3 for GMN, GGN and ASN.

Lemma 1. When $w_k(n)$ are i.i.d. Gaussian mixture random variables, $\mathcal{M}_w(p)$ and $\mathcal{M}_w(2p)$ can be provided as

$$\mathcal{M}_w(p) = \sum_{i=1}^U \frac{b_i}{\sqrt{\pi}} \Gamma\left(\frac{p+1}{2}\right) \left(\sqrt{2\sigma_i^2}\right)^p \tag{23}$$

$$\mathcal{M}_w(2p) = \sum_{i=1}^U \frac{b_i}{\sqrt{\pi}} \Gamma\left(\frac{2p+1}{2}\right) \left(\sqrt{2\sigma_i^2}\right)^{2p} \tag{24}$$

Proof. See Appendix 7. □

Lemma 2. When $w_k(n)$ follows generalized Gaussian distribution, $\mathcal{M}_w(p)$ and $\mathcal{M}_w(2p)$ can be expressed as

$$\mathcal{M}_w(p) = \frac{|A(\beta, \sigma_z)|^p \Gamma\left(\frac{p+1}{\beta}\right)}{\Gamma\left(\frac{1}{\beta}\right)} \tag{25}$$

$$\mathcal{M}_w(2p) = \frac{|A(\beta, \sigma_z)|^{2p} \Gamma\left(\frac{2p+1}{\beta}\right)}{\Gamma\left(\frac{1}{\beta}\right)} \tag{26}$$

Proof. See Appendix 8. □

Lemma 3. When $w_k(n)$ is characterized by alpha-stable distribution, $\mathcal{M}_w(p)$ and $\mathcal{M}_w(2p)$ can be given by

$$\mathcal{M}_w(p) = \frac{2^{p+1} \Gamma\left(\frac{p+1}{2}\right) \Gamma(-p/\alpha)}{\alpha \sqrt{\pi} \Gamma(-p/2)} \gamma^{p/\alpha} \tag{27}$$

$$\mathcal{M}_w(2p) = \frac{2^{2p+1} \Gamma\left(\frac{2p+1}{2}\right) \Gamma(-2p/\alpha)}{\alpha \sqrt{\pi} \Gamma(-2p/2)} \gamma^{2p/\alpha} \tag{28}$$

Proof. See Appendix 9. □

Based on these results, the mean and variance of \mathcal{T}_{SO} under \mathcal{H}_0 can be provided as

$$\mathbb{E}\{\mathcal{T}_{SO}|\mathbf{H}_0\} = \sum_{k=1}^K \varpi_k \exp\left(\frac{\mathbb{V}\{\mathcal{F}_k|\mathcal{H}_0\}}{2c^2} - \frac{\mathbb{E}\{\mathcal{F}_k|\mathbf{H}_0\}}{c}\right) \tag{29}$$

$$\begin{aligned} \mathbb{V}\{\mathcal{T}_{SO}|\mathcal{H}_0\} &= \sum_{k=1}^K \varpi_k^2 \exp\left(\frac{\mathbb{V}\{\mathcal{F}_k|\mathcal{H}_0\}}{c^2} - \frac{2\mathbb{E}\{\mathcal{F}_k|\mathcal{H}_0\}}{c}\right) \\ &\quad \times \left(\exp\left(\frac{\mathbb{V}\{\mathcal{F}_k|\mathbf{H}_0\}}{c^2}\right) - 1\right) \end{aligned} \tag{30}$$

Based on the Central Limit Theorem (CLT) for sufficiently large N , \mathcal{T}_{SO} approximately follows Gaussian distribution. Therefore, the false alarm probability \mathcal{P}_f can be given by

$$\mathcal{P}_f = 1 - \mathbb{Q}\left(\frac{\Psi - \mathbb{E}\{\mathcal{T}_{SO}|\mathbf{H}_0\}}{\sqrt{\mathbb{V}\{\mathcal{T}_{SO}|\mathcal{H}_0\}}}\right) \tag{31}$$

Therefore, the detection threshold for a given \mathcal{P}_f can be given as

$$\Psi = \mathbb{Q}^{-1}(1 - \mathcal{P}_f) \sqrt{\mathbb{V}\{\mathcal{T}_{SO}|\mathcal{H}_0\}} + \mathbb{E}\{\mathcal{T}_{SO}|\mathcal{H}_0\} \tag{32}$$

From (32), the detection threshold Ψ is simply a function of \mathcal{P}_f and the parameters N , K and $\mathcal{M}_w(p)$. The first two moments of $w_k(n)$ under H_0 , i.e. $\mathcal{M}_w(p)$ and $\mathcal{M}_w(2p)$ depend on the parameters of the noise distribution [36, 37].

4.2. Detection probability

Similar to false alarm probability, the distribution of \mathcal{T}_{SO} under the \mathcal{H}_1 hypotheses can be approximated by a Gaussian distribution. Under the hypothesis \mathcal{H}_1 , we let

$$\mathcal{F}_k|\mathbf{H}_1 = \frac{1}{N} \sum_{n=1}^N (1 - e^{-\lambda n}) |x_k(n)|^p \tag{33}$$

and then

$$\mathcal{T}_{SO}|\mathcal{H}_1 = \sum_{k=1}^K \varpi_k \exp\left(-\frac{\mathcal{F}_k|\mathcal{H}_1}{c}\right) \tag{34}$$

Let us now study the mean and variance of \mathcal{F}_k under \mathcal{H}_1 in Proposition 2.

Proposition 2. The mean and variance of \mathcal{F}_k under \mathcal{H}_1 can be provided as

$$\begin{aligned} \mathbb{E}\{\mathcal{F}_k|\mathcal{H}_1\} &= \frac{1}{N} \left(N - \frac{e^{-\lambda} - e^{-\lambda(N+1)}}{1 - e^{-\lambda}} \right) \\ &\quad \times \left(\mathcal{M}_w(p) + \frac{p(p-1)}{2} \sigma_{s_k}^2 \mathcal{M}_w(p-2) \right) \end{aligned} \tag{35}$$

$$\begin{aligned} \mathbb{V}\{\mathcal{F}_k|\mathcal{H}_1\} &= \frac{1}{N^2} \left(N + \frac{e^{-2\lambda} - e^{-2\lambda(N+1)}}{1 - e^{-2\lambda}} - 2 \frac{e^{-\lambda} - e^{-\lambda(N+1)}}{1 - e^{-\lambda}} \right) \\ &\quad \times \left(\mathcal{M}_w(2p) - \mathcal{M}_w^2(p) + p(2p-1) \sigma_{s_k}^2 \mathcal{M}_w(2p-2) \right. \\ &\quad \left. - p(p-1) \sigma_{s_k}^2 \mathcal{M}_w(p) \mathcal{M}_w(p-2) \right) \end{aligned} \tag{36}$$

Proof. See Appendix 10. □

Next, the mean and variance of \mathcal{T}_{SO} under \mathcal{H}_1 can be provided as

$$\mathbb{E}\{\mathcal{T}_{\text{SO}}|\mathbf{H}_1\} = \sum_{k=1}^K \varpi_k \exp\left(\frac{\mathbb{V}\{\mathcal{T}_k|\mathbf{H}_1\}}{2c^2} - \frac{\mathbb{E}\{\mathcal{T}_k|\mathbf{H}_1\}}{c}\right) \quad (37)$$

$$\begin{aligned} \mathbb{V}\{\mathcal{T}_{\text{SO}}|\mathbf{H}_1\} &= \sum_{k=1}^K \varpi_k^2 \exp\left(\frac{\mathbb{V}\{\mathcal{T}_k|\mathcal{H}_1\}}{c^2} - \frac{2\mathbb{E}\{\mathcal{T}_k|\mathbf{H}_1\}}{c}\right) \\ &\times \left(\exp\left(\frac{\mathbb{V}\{\mathcal{T}_k|\mathcal{H}_1\}}{c^2}\right) - 1\right) \end{aligned} \quad (38)$$

We again approximate the distribution of \mathcal{T}_{SO} to be Gaussian with sufficiently large N according to CLT, and have

$$\mathcal{P}_d = 1 - \mathcal{Q}\left(\frac{\Psi - \mathbb{E}\{\mathcal{T}_{\text{SO}}|\mathbf{H}_1\}}{\sqrt{\mathbb{V}\{\mathcal{T}_{\text{SO}}|\mathcal{H}_1\}}}\right) \quad (39)$$

In (39), the approximate analytical expressions of the detection probability can be obtained using the central limit theorem. From the formula, the \mathcal{P}_d increases linearly with the number of samples and receiver antenna. This is because the test statistic is very similar to Gaussian processes for large N and K . However, it is very difficult to find the exact \mathcal{P}_d due to the complexity of the function. Therefore, the detection probability will be obtained by approximation and Monte Carlo simulation.

5. Numerical results and discussion

In this section, we will evaluate the proposed scheme for randomly arriving primary signals under non-Gaussian noise in UAV communication. The detection performance of the proposed scheme is examined in terms of the Receiver Operating Characteristics (ROC) and the correct detection probability versus transmit MSNR (PTR). The transmit MSNR is defined by the ratio of the average transmit signal power to the average noise power as $\mathbb{E}\{\|s(n)\|^2\} / \sigma_w^2$. The variance of noise σ_w^2 is set to the dispersion parameter γ in the ASN model. Based on the simulation model, the main simulation parameters are considered as follows. For the large-scale fading, the path loss exponents of the LoS and NLoS are $\Delta_L = 2$ and $\Delta_N = 4$, respectively. Meanwhile, the path loss factors for the LoS and NLoS are $\psi_L = 0$ dB and $\psi_N = -20$ dB. The noise parameters are set to $\beta = 1.1$, $b_1 = 0.999$, $\sigma_2^2/\sigma_1^2 = 60$, $\alpha = 1.7$. In addition, the environment constants are set as $A = 9.6$ and $B = 0.16$. The small-scale fading is Nakagami-m fading with $m_L = 3$, $m_N = 1$. The height of the UAV is 200 m, and the radius of plan is 240 m. Each simulation result is based on 10000 trials.

Figs. 2–3 show the ROC curves and the PTR curves of the proposed scheme based on p -norm for different values of p . We set Transmit MSNR as 41 dB, 41 dB and 44 dB for GNN, GMN, ASN in Fig. 2. In Fig. 3, the number of received samples N are set $N = 300$, $N = 200$ and $N = 300$ for GNN, GMN, ASN. From Figs. 2–3, it is clear that the detection performance on the proposed scheme is dependent on the value of the parameter p and that the proposed scheme performs better for different values of p . We set the parameter p as 0.5, 1.0 and 0.2 for GNN, GMN, ASN in the subsequent simulations.

In Fig. 4 and Fig. 5, we show the ROC curves and the PTR curves for the number of antennas K , respectively. The curves are plotted for the following parameters: $N = 200$, and transmit MSNR are 39 dB, 41 dB and 41 dB for GNN, GMN, ASN in Fig. 4. The number of received samples N are set as $N = 600$, $N = 300$ and $N = 200$ for GNN, GMN, ASN in Fig. 5. In Fig. 4, we can see that the detection performance of the proposed scheme improves when the number of antennas K increases. For example, when the additive noise is GNN, the probability of detection is nearly 90% at $\mathcal{P}_f = 0.1$ and $K = 5$, and the probability of detection is close to 80% at $\mathcal{P}_f = 0.1$ and $K = 4$. Correspondingly, the detection probability is improved with the increase of K in Fig. 5. Furthermore, it can be clearly

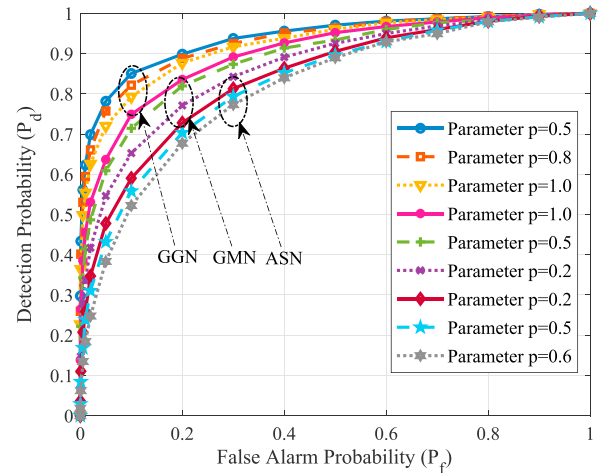


Fig. 2. ROC curves for proposed scheme with different value of p .

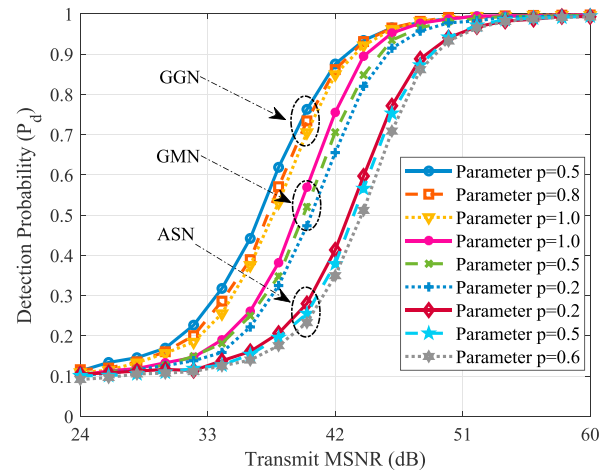


Fig. 3. PTR curves for proposed scheme with different value of p .

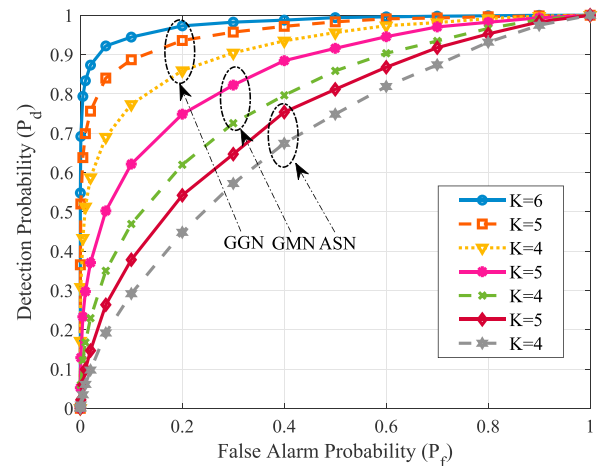


Fig. 4. ROC curves for proposed scheme with different values of K .

seen in Fig. 5 that a significant improvement in the detection performance results from increasing transmit MSNR.

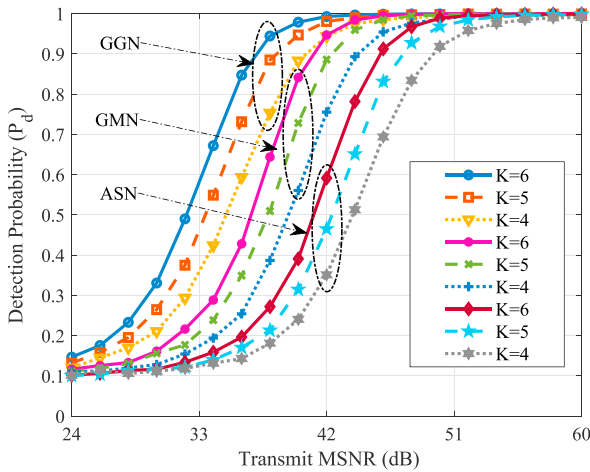


Fig. 5. PTR curves for proposed scheme with different values of K .

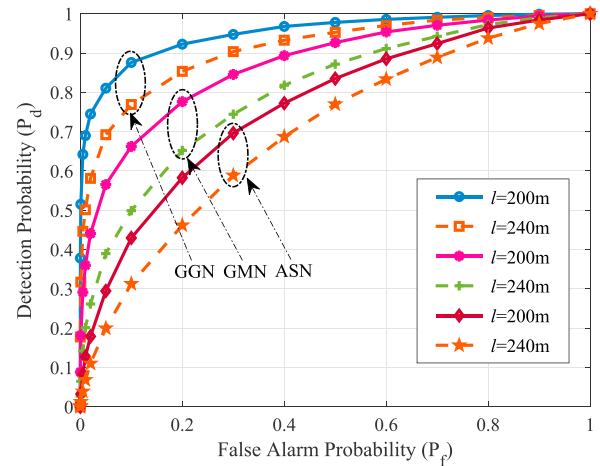


Fig. 8. ROC curves for the proposed scheme with different heights of the UAV.

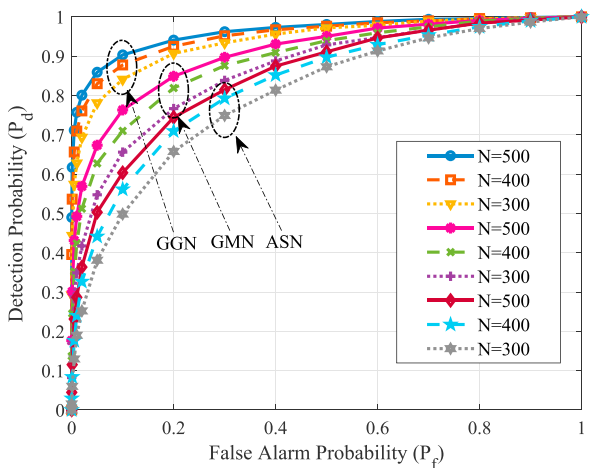


Fig. 6. ROC curves for proposed scheme with different values of N .

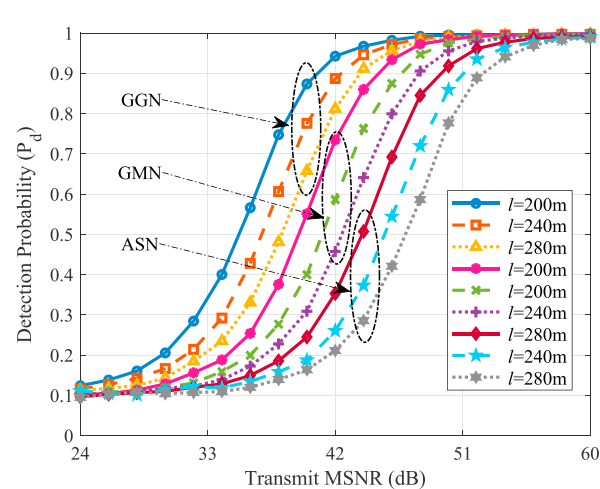


Fig. 9. PTR curves for the proposed scheme with different heights of the UAV.

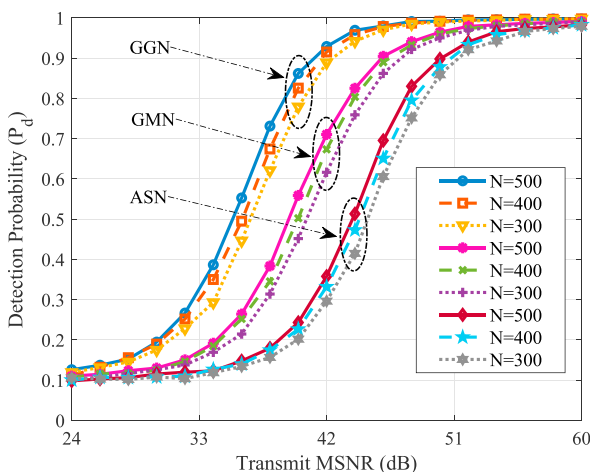


Fig. 7. PTR curves for proposed scheme with different values of N .

To evaluate the effect of the number of received samples N , Figs. 6–7 present the ROC curves and the PTR curves for different sample values of N under GMN, GGN and ASN, respectively. We set transmit MSNR as

41 dB, 40 dB and 43 dB for GGN, GMN, ASN in Fig. 6. In Fig. 7, the number of antennas K are set to $K = 4$, $K = 3$ and $K = 3$. From Figs. 6–7, we can see that the performance of the proposed scheme is different for the number of received samples N . The detection performance of the proposed scheme is positively correlated to the number of signal samples.

Figs. 8–9 give the ROC curves and PTR curves for different the height of the UAV in the presence of non-Gaussian noise. We set transmit MSNR as 40 dB, 41 dB and 43 dB for GGN, GMN, ASN in Fig. 8. In Fig. 9, the number of samples N are $N = 550$, $N = 200$ and $N = 200$ for GGN, GMN, ASN. According to Figs. 8–9, we can see that the performance of the proposed scheme is sensitive to the height of the UAV ℓ . The detection performance degrades with the increase of the height of UAV ℓ . This is mainly because the path loss increases with the increase of the height of UAV, which leads to the degradation of the detection performance of the proposed method.

In order to evaluate the performance of the proposed scheme in comparison with Multiple-antenna Linearly Weighted detector in Ref. [24], we depict the PTR curves for $P_f = 0.1$ in Fig. 10. The remaining parameters are set as follows: $\beta = 1.1$, $b_1 = 0.999$, $\sigma_2^2/\sigma_1^2 = 100$ and $\alpha = 1.8$. The number of received samples N are set as $N = 300$, $N = 200$ and $N = 300$ for GGN, GMN, ASN. It can be seen from Fig. 10 that the proposed

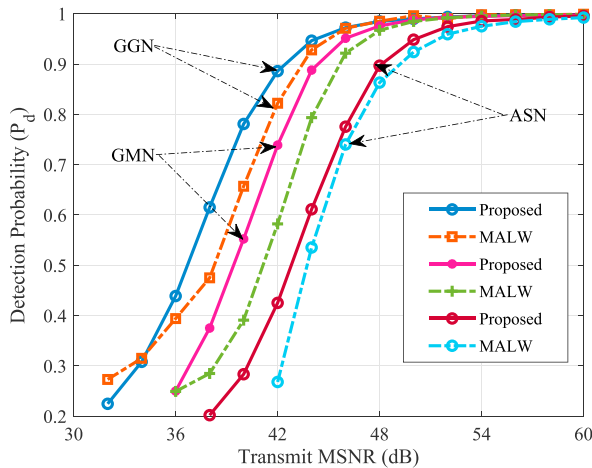


Fig. 10. PTR curves for the proposed scheme, p -Norm and MALW detector.

scheme outperforms the MALW detector in the presence of non-Gaussian noise for the given false alarm probability. For example, when \mathcal{P}_f is fixed at 0.1, the detection probability gain of the proposed scheme is about 10% for the MALW detectors with transmit MSNR = 42 dB.

6. Conclusion

In this paper, we have investigated the detection of primary signals

Appendix

7. Proof of Lemma 1

Under \mathcal{H}_0 hypothesis, assume that $w_k(n)$ are i.i.d. And Gaussian mixture random variables, the moments of $|w_k(n)|^p$ can be expressed as

$$\begin{aligned} \mathcal{M}_w(p) &= \mathbb{E}\{|w_k(n)|^p\} = \int_{-\infty}^{\infty} |w_k(n)|^p f_z(w_k(n)) dw_k(n) = \int_{-\infty}^{\infty} |w_k(n)|^p \sum_{i=1}^U \frac{b_i}{\sqrt{2\pi\sigma_i^2}} \exp\left(-\frac{|w_k(n)|^2}{2\sigma_i^2}\right) dw_k(n) \\ &= \sum_{i=1}^U \frac{b_i}{\sqrt{2\pi\sigma_i^2}} \int_{-\infty}^{\infty} |w_k(n)|^p \exp\left(-\frac{|w_k(n)|^2}{2\sigma_i^2}\right) dw_k(n) = \sum_{i=1}^U \frac{b_i}{\sqrt{\pi}} \Gamma\left(\frac{p+1}{2}\right) \left(\sqrt{2\sigma_i^2}\right)^p \end{aligned} \tag{40}$$

where $\Gamma(\cdot)$ denotes the Gamma function.

Then, the moments of $|w_k(n)|^{2p}$ under \mathcal{H}_0 hypothesis can be obtained as

$$\begin{aligned} \mathcal{M}_w(2p) &= \mathbb{E}\{|w_k(n)|^{2p}\} = \int_{-\infty}^{\infty} |w_k(n)|^{2p} f_z(w_k(n)) dw_k(n) = \int_{-\infty}^{\infty} |w_k(n)|^{2p} \sum_{i=1}^U \frac{b_i}{\sqrt{2\pi\sigma_i^2}} \exp\left(-\frac{|w_k(n)|^2}{2\sigma_i^2}\right) dw_k(n) \\ &= \sum_{i=1}^U \frac{b_i}{\sqrt{2\pi\sigma_i^2}} \int_{-\infty}^{\infty} |w_k(n)|^{2p} \exp\left(-\frac{|w_k(n)|^2}{2\sigma_i^2}\right) dw_k(n) = \sum_{i=1}^U \frac{b_i}{\sqrt{\pi}} \Gamma\left(\frac{2p+1}{2}\right) \left(\sqrt{2\sigma_i^2}\right)^{2p} \end{aligned} \tag{41}$$

8. Proof of Lemma 2

Under \mathcal{H}_0 hypothesis, suppose that $w_k(n)$ are i.i.d. And generalized Gaussian random variables with P.D.F., i.e.

$$f(w_k) = \frac{1}{2\Gamma\left(\frac{1}{\beta}\right)A(\beta, \sigma_w)} \exp\left(-\left|\frac{w_k}{A(\beta, \sigma_w)}\right|^\beta\right) \tag{42}$$

Then, the first and second moments of $|w_k(n)|^p$, under the \mathcal{H}_0 hypothesis, are given by

when they are corrupted by additive non-Gaussian noise and arrive randomly during the spectrum sensing period in green UAV communication. We have proposed an improved p -norm-based spectrum and energy-efficient spectrum sensing scheme. The approximate analytical expressions for false alarm probability, decision threshold, and detection probability of the proposed scheme have been derived in the presence of the GMD, GGD and ASN. Numerical simulation results have shown that the proposed scheme achieved much better performance than the MALW. In addition, we have observed that the detection performance of the proposed scheme increases with the increase of transmit MSNR, the number of samples and the number of receiver antennas.

Declaration of competing interest

The authors declare that they have no known competing financial interests or personal relationships that could have appeared to influence the work reported in this paper.

Acknowledgements

This work was supported by the National Natural Science Foundation of China under Grant 62071364 and 62231027, China Postdoctoral Science Foundation under Grant 2022M722504, in part by the Key Research and Development Program of Shaanxi under Grant 2023-YBGY-249, in part by the Fundamental Research Funds for the Central Universities under Grant XJSJ23090 and KYFZ23001.

$$\begin{aligned} \mathcal{M}_w(p) &= \mathbb{E}\{|w_k(n)|^p\} = \int_{-\infty}^{\infty} |w_k(n)|^p f_z(w_k(n)) dw_k(n) = \int_{-\infty}^{\infty} |w_k(n)|^p \frac{1}{2\Gamma(\frac{1}{\beta})A(\beta, \sigma_w)} \times \exp\left(-\left|\frac{w_k(n)}{A(\beta, \sigma_w)}\right|^\beta\right) dw_k(n) \\ &= \frac{1}{2\Gamma(\frac{1}{\beta})A(\beta, \sigma_w)} \int_{-\infty}^{\infty} |w_k(n)|^p \times \exp\left(-\left|\frac{w_k(n)}{A(\beta, \sigma_w)}\right|^\beta\right) dw_k(n) = \frac{|A(\beta, \sigma_w)|^p \Gamma(\frac{p+1}{\beta})}{\Gamma(\frac{1}{\beta})} \end{aligned} \tag{43}$$

$$\begin{aligned} \mathcal{M}_w(2p) &= \mathbb{E}\{|w_k(n)|^{2p}\} = \int_{-\infty}^{\infty} |w_k(n)|^{2p} f_z(w_k(n)) dw_k(n) = \int_{-\infty}^{\infty} |w_k(n)|^{2p} \frac{1}{\Gamma(\frac{1}{\beta})A(\beta, \sigma_w)} \times \exp\left(-\left|\frac{w_k(n)}{A(\beta, \sigma_w)}\right|^\beta\right) dw_k(n) \\ &= \frac{1}{\Gamma(\frac{1}{\beta})A(\beta, \sigma_w)} \int_{-\infty}^{\infty} |w_k(n)|^{2p} \times \exp\left(-\left|\frac{w_k(n)}{A(\beta, \sigma_w)}\right|^\beta\right) dw_k(n) = \frac{|A(\beta, \sigma_w)|^{2p} \Gamma(\frac{2p+1}{\beta})}{\Gamma(\frac{1}{\beta})} \end{aligned} \tag{44}$$

9. Proof of Lemma 3

According to Eq. (11) and Eq. (12) in Ref. [15], the first and second moments of $|w_k(n)|^p$, under the \mathcal{H}_0 hypothesis, are given as

$$\mathcal{M}_w(p) = \mathbb{E}\{|w_k(n)|^p\} = C(p, \alpha) \gamma^{p/\alpha} = \frac{2^{p+1} \Gamma(\frac{p+1}{2}) \Gamma(-p/\alpha)}{\alpha \sqrt{\pi} \Gamma(-p/2)} \gamma^{p/\alpha} \tag{45}$$

$$\mathcal{M}_w(2p) = \mathbb{E}\{|w_k(n)|^{2p}\} = C(2p, \alpha) \gamma^{2p/\alpha} = \frac{2^{2p+1} \Gamma(\frac{2p+1}{2}) \Gamma(-2p/\alpha)}{\alpha \sqrt{\pi} \Gamma(-2p/2)} \gamma^{2p/\alpha} \tag{46}$$

10. Proof of Proposition 2

By using Lemma 5, the mean of \mathcal{F}_k under \mathcal{H}_1 can be calculated as

$$\mathbb{E}\{\mathcal{F}_k | \mathbf{H}_1\} = \mathbb{E}\left\{\sum_{n=1}^N (1 - e^{-\lambda n}) |h_{qk} s_q(n) + w_k(n)|^p\right\} = \frac{1}{N} \left(N - \frac{e^{-\lambda} - e^{-\lambda(N+1)}}{1 - e^{-\lambda}}\right) \mathbb{E}\{|h_{qk} s_q(n) + w_k(n)|^p\} \tag{47}$$

By using the generalized binomial theorem, $\mathbb{E}\left\{\left|\sum_{q=1}^Q h_{qk} s_q(n) + w_k(n)\right|^p\right\}$ can be approximately expressed as

$$\begin{aligned} \mathbb{E}\left\{\left|\sum_{q=1}^Q h_{qk} s_q(n) + w_k(n)\right|^p\right\} &\approx \mathbb{E}\left\{|w_k(n)|^p + \frac{p(p-1)}{2} \left|\sum_{q=1}^Q h_{qk} s_q(n)\right|^2 |w_k(n)|^{p-2}\right\} = \mathbb{E}\{|w_k(n)|^p\} + \frac{p(p-1)}{2} \sigma_{s_k}^2 \mathbb{E}\{|w_k(n)|^{p-2}\} \\ &= \mathcal{M}_w(p) + \frac{p(p-1)}{2} \sigma_{s_k}^2 \mathcal{M}_w(p-2) \end{aligned} \tag{48}$$

where $\sigma_{s_k}^2 = \mathbb{E}\left\{\left|\sum_{q=1}^Q h_{qk} s_q(n)\right|^2\right\}$.

Substituting (48) into (47), the mean of \mathcal{F}_k under \mathcal{H}_1 can be expressed as

$$\mathbb{E}\{\mathcal{F}_k | \mathbf{H}_1\} = \frac{1}{N} \left(N - \frac{e^{-\lambda} - e^{-\lambda(N+1)}}{1 - e^{-\lambda}}\right) \times \left(\mathcal{M}_w(p) + \frac{p(p-1)}{2} \sigma_{s_k}^2 \mathcal{M}_w(p-2)\right) \tag{49}$$

The variance of \mathcal{F}_k under \mathcal{H}_1 can be expressed as

$$\begin{aligned} \mathbb{V}\{\mathcal{F}_k | \mathbf{H}_1\} &= \left(N + \frac{e^{-2\lambda} - e^{-2\lambda(N+1)}}{1 - e^{-2\lambda}} - 2 \frac{e^{-\lambda} - e^{-\lambda(N+1)}}{1 - e^{-\lambda}}\right) \times \frac{1}{N^2} \mathbb{V}\{|x_k(n)|^p\} \\ &= \left(N + \frac{e^{-2\lambda} - e^{-2\lambda(N+1)}}{1 - e^{-2\lambda}} - 2 \frac{e^{-\lambda} - e^{-\lambda(N+1)}}{1 - e^{-\lambda}}\right) \times \frac{1}{N^2} (\mathbb{E}\{|x_k(n)|^{2p}\} - \mathbb{E}^2\{|x_k(n)|^p\}) \end{aligned} \tag{50}$$

$$\begin{aligned} \mathbb{V}\{|x_k(n)|^p\} &= \mathbb{E}\{|x_k(n)|^{2p}\} - \mathbb{E}^2\{|x_k(n)|^p\} = \mathbb{E}\left\{\left|\sum_{q=1}^Q h_{qk}s_q(n) + w_k(n)\right|^{2p}\right\} - \mathbb{E}^2\left\{\left|\sum_{q=1}^Q h_{qk}s_q(n) + w_k(n)\right|^p\right\} \\ &\approx \mathbb{E}\left\{|w_k(n)|^{2p} + \frac{2p(2p-1)}{2}\left|\sum_{q=1}^Q h_{qk}s_q(n)\right|^2 |w_k(n)|^{2p-2}\right\} - \mathbb{E}^2\left\{|w_k(n)|^p + \frac{p(p-1)}{2}\left|\sum_{q=1}^Q h_{qk}s_q(n)\right|^2 |w_k(n)|^{p-2}\right\} \\ &= \mathcal{M}_w(2p) + p(2p-1)\sigma_{s_k}^2 \mathcal{M}_w(2p-2) - \mathcal{M}_w^2(p) - p(p-1)\sigma_{s_k}^2 \mathcal{M}_w(p)\mathcal{M}_w(p-2) \end{aligned} \quad (51)$$

According to (50) and (51), the variance of \mathcal{F}_k under \mathcal{H}_1 can be expressed as

$$\mathbb{V}\{\mathcal{F}_k|\mathcal{H}_1\} = \frac{1}{N^2} \left(N + \frac{e^{-2\lambda} - e^{-2\lambda(N+1)}}{1 - e^{-2\lambda}} - 2 \frac{e^{-\lambda} - e^{-\lambda(N+1)}}{1 - e^{-\lambda}} \right) \times \left(\mathcal{M}_w(2p) - \mathcal{M}_w^2(p) + p(2p-1)\sigma_{s_k}^2 \mathcal{M}_w(2p-2) - p(p-1)\sigma_{s_k}^2 \mathcal{M}_w(p)\mathcal{M}_w(p-2) \right) \quad (52)$$

References

[1] T. Zhang, Y. Wang, Y. Liu, W. Xu, A. Nallanathan, Cache-enabling UAV communications: network deployment and resource allocation, *IEEE Trans. Wireless Commun.* 19 (11) (2020) 7470–7483.

[2] X. Pang, G. Gui, N. Zhao, W. Zhang, Y. Chen, Z. Ding, F. Adach, Uplink precoding optimization for NOMA cellular-connected UAV networks, *IEEE Trans. Commun.* 68 (2) (2020) 1271–1283.

[3] H. Song, L. Liu, S., M. Pudlewski, E.S. Bentley, Random network coding enabled routing protocol in unmanned aerial vehicle networks, *IEEE Trans. Wireless Commun.* 19 (12) (2020) 8382–8395.

[4] W. Sun, N. Xu, L. Wang, H. Zhang, Y. Zhang, Dynamic digital twin and federated learning with incentives for air-ground networks, *IEEE Trans. Netw. Sci. Eng.* 9 (1) (2022) 321–333.

[5] W. Sun, P. Wang, N. Xu, G. Wang, Y. Zhang, Dynamic digital twin and distributed incentives for resource allocation in aerial-assisted internet of vehicles, *IEEE Internet Things J.* 9 (8) (2022) 5839–5852.

[6] S. Mao, S. Leng, S. Maharjan, Y. Zhang, Energy efficiency and delay tradeoff for wireless powered mobile-edge computing systems with multi-access schemes, *IEEE Trans. Wireless Commun.* 19 (3) (2020) 1855–1867.

[7] Y. Dai, K. Zhang, S. Maharjan, Y. Zhang, Edge intelligence for energy-efficient computation offloading and resource allocation in 5G beyond, *IEEE Trans. Veh. Technol.* 69 (10) (2020) 12175–12186.

[8] M.H.T. Nguyen, E. Garcia-Palacios, T. Do-Duy, L.D. Nguyen, S.T. Mai, T.Q. Duong, Spectrum-sharing UAV-assisted mission-critical communication: learning-aided real-time optimisation, *IEEE Access* 9 (2021) 11622–11632.

[9] A.A. Khuwaja, Y. Chen, N. Zhao, M.-S. Alouini, P. Dobbins, A survey of channel modeling for UAV communications, *IEEE Commun. Surveys Tuts.* 20 (4) (2018) 2804–2821.

[10] H.S. Chen, W. Gao, D.G. Daut, Signature based spectrum sensing algorithms for IEEE 802.22 WRAN, in: *Proceedings of the 2007 IEEE International Conference on Communications, IEEE, 2007*, pp. 6487–6492.

[11] B. Li, M. Sun, X. Li, A. Nallanathan, C. Zhao, Energy detection based spectrum sensing for cognitive radios over time-frequency doubly selective fading channels, *IEEE Trans. Signal Process.* 63 (2) (2015) 402–417.

[12] S. Chaudhari, et al., Performance evaluation of cyclostationary-based cooperative sensing using field measurements, *IEEE Trans. Veh. Technol.* 65 (4) (2016) 1982–1997.

[13] C. Liu, J. Wang, X. Liu, Y.-C. Liang, Maximum eigenvalue-based goodness-of-fit detection for spectrum sensing in cognitive radio, *IEEE Trans. Veh. Technol.* 68 (8) (2019) 1168–1184.

[14] A. Chen, Z. Shi, Z. He, A real-valued weighted covariance-based detection method for cognitive radio networks with correlated multiple antennas, *IEEE Commun. Lett.* 22 (11) (2018) 2290–2293.

[15] X. Zhu, W. Zhu, B. Champagne, Spectrum sensing based on fractional lower order moments for cognitive radios in alpha-stable distributed noise, *Signal Process.* 111 (2014) 94–105.

[16] F. Moghimi, A. Nasri, R. Schober, Adaptive L_p -norm spectrum sensing for cognitive radio networks, *IEEE Trans. Commun.* 59 (7) (2011) 1934–1945.

[17] V. Kostylev, I. Gres, Characteristics of p-norm signal detection in Gaussian mixture noise, *IEEE Trans. Veh. Technol.* 67 (4) (2018) 2973–2981.

[18] T. Wimalajeewa, P.K. Varshney, Polarity-coincidence-array based spectrum sensing for multiple antenna cognitive radios in the presence of non-Gaussian noise, *IEEE Trans. Wireless Commun.* 10 (7) (2011) 2362–2371.

[19] M. Karimzadeh, A.M. Rabiei, A. Olfat, Soft-limited polarity-coincidence-array spectrum sensing in the presence of non-Gaussian noise, *IEEE Trans. Veh. Technol.* 66 (2) (2017) 1418–1427.

[20] N.C. Beaulieu, Y. Chen, Improved energy detectors for cognitive radios with randomly arriving or departing primary users, *IEEE Signal Process. Lett.* 17 (10) (2010) 867–870.

[21] T. Duzenli, O. Akay, A new spectrum sensing strategy for dynamic primary users in cognitive radio, *IEEE Commun. Lett.* 20 (4) (2016) 752–755.

[22] W.L. Chin, J.M. Li, H.H. Wang, Low-complexity energy detection for spectrum sensing with random arrivals of primary users, *IEEE Trans. Veh. Technol.* 65 (2) (2016) 947–952.

[23] M. Deng, B.J. Hu, X. Li, Adaptive weighted sensing with simultaneous transmission for dynamic primary user traffic, *IEEE Trans. Commun.* 65 (3) (2017) 992–1004.

[24] J. Wang, R. Chen, J. Huang, F. Shu, Z. Chen, G. Min, Multiple-antenna spectrum sensing method with random arrivals of primary users, *IEEE Trans. Veh. Technol.* 67 (9) (2018) 8978–8983.

[25] W. Xu, S. Wang, S. Yan, J. He, An efficient wideband spectrum sensing algorithm for unmanned aerial vehicle communication networks, *IEEE Internet Things J.* 6 (2) (2019) 1768–1780.

[26] F. Shen, G. Ding, Z. Wang, Q. Wu, UAV-based 3D spectrum sensing in spectrum-heterogeneous networks, *IEEE Trans. Veh. Technol.* 68 (6) (2019) 5711–5722.

[27] X. Liu, M. Guan, X. Zhang, H. Ding, Spectrum sensing optimization in an UAV-based cognitive radio, *IEEE Access* 6 (2018) 44002–44009.

[28] A.M. Almasoud, A.E. Kamal, Data dissemination in IoT using a cognitive UAV, *IEEE Trans. Cogn. Commun. Netw.* 5 (4) (2019) 849–862.

[29] W. Mei, R. Zhang, UAV-sensing-assisted cellular interference coordination: a cognitive radio approach, *IEEE Wireless Commun. Lett.* 9 (6) (2020) 799–803.

[30] B. Shang, Y. Yi, L. Liu, Spectrum sharing for UAV communications: spatial spectrum sensing and open issues, *IEEE Veh. Technol. Mag.* 15 (2) (2020) 104–112.

[31] M. Liu, B. Li, Y. Chen, Z. Yang, N. Zhao, P. Liu, F. Gong, Location parameter estimation of moving aerial target in space-air-ground integrated networks-based IoV, *IEEE Internet Things J.* 9 (8) (2022) 5696–5707.

[32] M. Liu, C. Liu, M. Li, Y. Chen, S. Zheng, N. Zhao, Intelligent passive detection of aerial target in space-air-ground integrated networks, *China Communications* 19 (1) (2022) 52–63.

[33] T. Hou, Y. Liu, Z. Song, X. Sun, Y. Chen, Multiple antenna aided NOMA in UAV networks: a stochastic geometry approach, *IEEE Trans. Commun.* 67 (2) (2019) 1031–1044.

[34] F. Li, X. Zhao, Block-structured compressed spectrum sensing with Gaussian mixture noise distribution, *IEEE Wireless Commun. Lett.* 8 (4) (2019) 1183–1186.

[35] S. Gurugopinath, R. Muralishankar, H.N. Shankar, Differential entropy-driven spectrum sensing under generalized Gaussian noise, *IEEE Commun. Lett.* 20 (7) (2016) 1321–1324.

[36] M. Liu, Z. Liu, W. Lu, Y. Chen, X. Gao, N. Zhao, Distributed few-shot learning for intelligent recognition of communication jamming, *IEEE J. Select. Topic. Signal Process.* 16 (3) (2022) 395–405.

[37] M. Liu, J. Wang, N. Zhao, Y. Chen, H. Song, R. Yu, Radio frequency fingerprint collaborative intelligent identification using incremental learning, *IEEE Trans. Netw. Sci. and Eng.* 9 (5) (2022) 3222–3233.